Chaotic and ballistic dynamics in time-driven quasiperiodic lattices

Thomas Wulf[1,*] and Peter Schmelcher[1,2,†]

[1]*Zentrum für Optische Quantentechnologien, Universität Hamburg, Luruper Chaussee 149, 22761 Hamburg, Germany*

[2]*The Hamburg Centre for Ultrafast Imaging, Universität Hamburg, Luruper Chaussee 149, 22761 Hamburg, Germany*

(Received 3 February 2016; published 21 April 2016)

We investigate the nonequilibrium dynamics of classical particles in a driven quasiperiodic lattice based on the Fibonacci sequence. An intricate transient dynamics of extraordinarily long ballistic flights at distinct velocities is found. We argue how these transients are caused and can be understood by a hierarchy of block decompositions of the quasiperiodic lattice. A comparison to the cases of periodic and fully randomized lattices is performed.

DOI: 10.1103/PhysRevE.93.042215

I. INTRODUCTION

One of the workhorses in the field of classical chaotic dynamics of time-driven setups are driven lattices, i.e., spatially periodic potentials subjected to a temporally periodic forcing. In particular, their resulting transport properties have received tremendous attention as they provide working principles for Brownian or molecular motors [1–9] or have even found direct technical applications, e.g., in particle species separation [10–13]. In terms of the direct experimental realization of such driven lattice potentials, cold atoms loaded into shaken optical lattices as generated by counter propagating laser beams have been shown to provide an ideal toolbox as they allow for precise control of the system parameters and thus for an experimental verification of many of the theoretically introduced concepts on ratchet transport [14–17].

An interesting aspect of driven lattice physics has been the effect of deviations from a purely periodic setup. Here, for coupled, dissipative systems it was shown how isolated impurities may stabilize soliton solutions [18,19] or how—more generally—the introduction of disorder initiates synchronization in the asymptotically reached state [20,21]. Recently, it was also demonstrated how disorder may lead to ordering, in the sense of increased autocorrelations and strongly peaked velocity distributions, even in Hamiltonian lattice systems [22]. At this point it is certainly worth mentioning that the two structurally limiting cases of strictly periodic and fully randomized lattices have, of course, also been investigated keenly in the quantum domain. Here the periodic regime is characterized by extended Bloch waves [23], whereas randomness is often accompanied by the celebrated Anderson localization effect [24]. In the quantum domain, however, a third form of spatial structure has also attracted considerable attention, namely quasiperiodic lattices, triggered particularly by the pioneering work of Shechtman *et al.* [25], where the possibility of long-range order even in the absence of translational symmetry was demonstrated. In fact, it was shown how quasiperiodicity leads here to a qualitatively new phenomenology compared to both the periodic and the random cases [26,27], specific examples being self-similar critical states or singularly continuous energy spectra [28,29].

In the classical regime, however, quasiperiodic lattices and their associated chaotic nonequilibrium dynamics have so far been largely unexplored. Shining light on this dynamics is the purpose of the present manuscript. To this end, we study periodically driven lattices built of individual scatterers which are arranged in a quasiperiodic, as compared to a periodic or randomized, manner. We hereby focus on quasiperiodicity as generated by the Fibonacci sequence, constituting one of the commonly studied implementations of quasiperiodicity [29]. Indeed, we showcase observables, in particular, the ballistic flight length distribution, where qualitative differences between the quasiperiodic and the periodic and random lattices are apparent. Specifically, we find velocity domains where particles perform exceptionally long ballistic flights, a feature shown to be absent in the randomized lattice and hence hinting at the high degree of long-range order in the Fibonacci chain [30–32]. We demonstrate how the quasiperiodic lattice can be decomposed into a hierarchy of building blocks, where each hierarchy is shown to naturally induce a set of Poincaré maps which describe the dynamics on increasingly larger length scales. By this approach, we are able to relate invariant subsets of the Poincaré maps corresponding to distinct hierarchical levels to the observed long ballistic flight events. Here we stress that the routinely employed analysis tools, in particular Poincaré surfaces of section, rely intrinsically on the driven systems periodicity. Hence, they cannot be applied straightforwardly to driven quasicrystalline systems, making their analysis and physical interpretation of obtained results a genuinely challenging prospect. For this reason, we believe that the introduced notion of a set of Poincaré maps, adapted specifically to the given quasiperiodic lattice, should be of conceptual interest in the investigation of the chaotic dynamics of aperiodic driven systems.

Our manuscript is structured as follows: In Sec. II we introduce the driven lattice Hamiltonian for the periodic, quasiperiodic, and randomized cases. In Sec. III, some basic notions of chaotic dynamics in driven lattices are introduced. Section IV contains a comparison of the flight length distributions for all three cases. These results are further analyzed in Sec. V and explained by means of a block decomposition of the Fibonacci lattice in Sec. VI. Finally, we provide our conclusions in Sec. VII.

*thomas.wulf@physnet.uni-hamburg.de

†peter.schmelcher@physnet.uni-hamburg.de

II. THE DRIVEN LATTICE HAMILTONIAN

Throughout this work we study the dynamics of noninteracting classical particles of equal mass m governed by the driven lattice Hamiltonian:

$$H(x,p,t) = \frac{p^2}{2m} + \sum_{n=1}^{\infty} V_n \Theta(l/2 - |x - X_n - d(t)|). \quad (1)$$

That is, the potential consists of a semi-infinite array of individual barriers of width l and site-dependent heights V_n. Furthermore, the barriers oscillate around their equilibrium positions $X_n \equiv n \times L$, where L denotes the lattice spacing, according to the driving law $d(t) = A\sin(\omega t)$ with driving amplitude A, driving frequency ω, and resulting temporal periodicity $T = 2\pi/\omega$. (Throughout the manuscript, initial conditions will be chosen randomly at large x, such that the boarders of the lattice are not reached within the simulation time.) Such a Hamiltonian may be seen as minimalistic model for time-dependent lattice systems as occurring in radiated semiconductors or in cold atom physics. The major advantage of it is that, via appropriate choices of the site dependent barrier heights V_n, different spatial structures of the lattice can be realized and dynamical processes occurring there can be analyzed and compared. We are interested here in three different types of lattices which will be shown to yield substantially different dynamical evolutions for particle ensembles. Specifically, these three cases are periodic lattices (PL), randomized lattices (RL), and quasiperiodic Fibonacci lattices (FL). Each of these can be realized by introducing two types of barriers denoted symbolically by $\mathcal{A}$ and $\mathcal{B}$. Barriers of different type are thereby distinguished by their height, i.e., V_n takes either of the two different values $V_\mathcal{A}$ or $V_\mathcal{B}$ throughout the lattice [see Fig. 1(a) for a sketch of the setup]. $\mathcal{A}$ and $\mathcal{B}$ barriers are then arranged in a periodic, quasiperiodic, or randomized manner:

$$\begin{aligned} &\text{PL: } V_n = V_\mathcal{A} \\ &\text{RL: } V_n = V_\mathcal{A}, \text{ for } \sigma_n = 1, \quad V_n = V_\mathcal{B} \text{ for } \sigma_n = 0 \\ &\text{FL: } V_n = V_\mathcal{A}, \text{ for } \mathcal{F}_n = 1, \quad V_n = V_\mathcal{B} \text{ for } \mathcal{F}_n = 0, \end{aligned} \quad (2)$$

where σ is a randomized sequence of zeros and ones. Contrarily, $\mathcal{F}$ is a quasiperiodic sequence, again of zeros and ones but whose elements $\mathcal{F}_n$ are arranged according to a construction principle based on the Fibonacci numbers (see, e.g., Ref. [32] for details), such that the first few elements are given by:

$$\mathcal{F} = 1\ 10\ 101\ 10110\ 10110101\ldots. \quad (3)$$

Interestingly, the Fibonacci sequence, although never periodically repeating, contains a plethora of structurally highly nontrivial properties, such as local parity symmetry on all scales [32], and has been the subject of intensive research in both physics [29,33] and mathematics [30,31].

III. MOTION IN PERIODIC, QUASIPERIODIC, AND RANDOMIZED DRIVEN LATTICES: BASIC CONCEPTS

In the periodic case, the setups mixed phase space can be visualized conveniently by the Poincaré surface of section (PSS). Here we denote velocities and phases $\phi \equiv (t \mod T)$ at positions $X^{\text{PSS}} = \{x, x = n \times L\}$ for $n \in \mathbb{N}$ [cf. Fig. 1(a)]. The extract of the resulting PSS for a PL, which is of relevance for the results presented in this manuscript, is shown in Fig. 1(b), revealing the typical ingredients: a "chaotic sea", regular or "ballistic" islands embedded in it, and, finally, invariant curves confining the chaotic sea at higher velocities (because of the time reversal symmetry of the used Hamiltonian, the PSS is mirror symmetric around $v = 0$). An exemplary trajectory of the PL with initial conditions belonging to the chaotic sea is depicted in Fig. 2(a) and shows a mostly erratic motion with frequent changes of magnitude and sign of the velocity, accompanied by phases of motion where its velocity only fluctuates slightly; see, e.g., the inset of Fig. 2(a). These "stickiness" events are known to be quite generic for Hamiltonian systems and, simply put, originate from the fact that a chaotic trajectory gets drawn in by the intricate network of stable and unstable fixed points surrounding a regular structure which borders the chaotic sea [34]. Furthermore, the maximal speed of a trajectory in the chaotic sea is denoted by $v^{\text{C}}_{\text{max}}$ [see the horizontal dashed lines in Fig. 1(b) and Fig. 2].

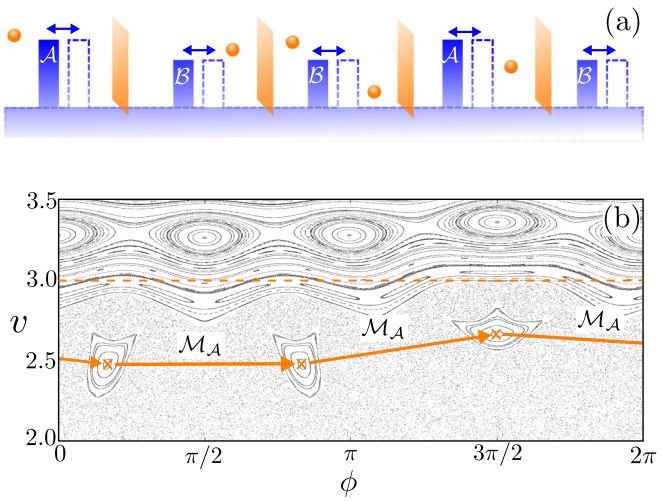

FIG. 1. (a) Sketch of a laterally oscillating lattice build of two barrier types $\mathcal{A}$ and $\mathcal{B}$ distinguished by their potential heights $V_\mathcal{A}$ and $V_\mathcal{B}$. Between consecutive barriers are the Poincaré surfaces (orange). (b) Extract of the Poincaré surface of section of a periodic lattice consisting only of $\mathcal{A}$-type barriers with $V_\mathcal{A} = 1.5$. The horizontal dashed line indicates the maximal velocity $v^{\text{C}}_{\text{max}}$ that particles can acquire in the chaotic sea. Also shown is the period three fixed point of the Poincaré map $\mathcal{M}_\mathcal{A}$ centering the three corresponding regular islands. Each arrow indicates one application of $\mathcal{M}_\mathcal{A}$ on a trajectory in the fixed point. Remaining parameters are $\omega = A = m = l = 1.0$ and $L = 5.0$.

For the randomized lattice, there is no such bound on the particle's energy and it is in fact expected that the RL features Fermi acceleration, as was demonstrated for comparable, randomized setups [35]. If we again consider an exemplary trajectory for the RL [Fig. 2(b)], then we see, somewhat analogously to the PL, an apparently irregular motion at velocities corresponding to the chaotic sea of the PL, which is interrupted by long unidirectional flights at higher velocities.

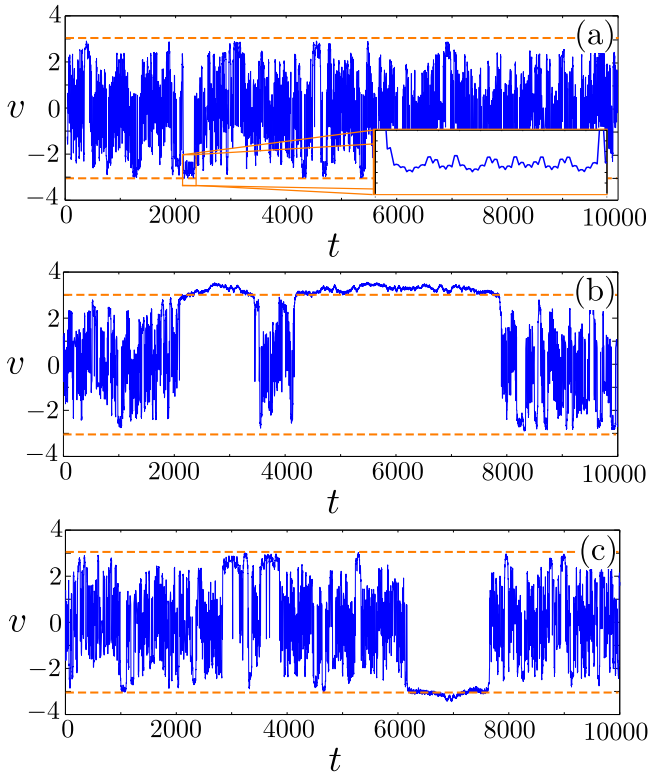

FIG. 2. Exemplary trajectories $v(t)$ for the periodic (a), randomized (b), and quasiperiodic lattices (c). In all three cases, the horizontal line denotes $\pm v^{\mathrm{C}}_{\mathrm{max}}$ [see Fig. 1(b)]. The inset in (a) shows a zoom into a typical stickiness event. Parameters are $V_{\mathcal{A}} = 1.5$ [same as in Fig. 1(b)] and $V_{\mathcal{B}} = 1.0$. Remaining parameters are the same as in Fig. 1.

A similar behavior can be observed for the sample trajectory in the quasiperiodic lattice [Fig. 2(c)], where again the particle motion at small velocities with $|v| \lesssim |v^{\mathrm{C}}_{\mathrm{max}}|$ is accompanied by large fluctuations in the velocity and is interrupted by long flights at higher velocities. Hence, at least from this simple analysis based on sample trajectories, it appears that differences in the dynamical properties of the three studied lattice types are manifest mostly in the dynamics at $|v| \gtrsim |v^{\mathrm{C}}_{\mathrm{max}}|$ rather than in the low-energy regime.

IV. FLIGHT LENGTHS IN PERIODIC, QUASIPERIODIC, AND RANDOMIZED DRIVEN LATTICES

We now focus on a systematic investigation of the question if and how any of the structural properties of the Fibonacci sequence translate into dynamical properties of the nonequilibrium dynamics of particles. As indicated above, a promising candidate for an effect where the periodic, randomized, and quasiperiodic lattices significantly differ from one another are long flight events at velocities $|v| \gtrsim |v^{\mathrm{C}}_{\mathrm{max}}|$. Here, a particle traverses many barriers and thus correlations between lattice sites even on large scales can be expected to play a role.

In order to investigate these long flight events quantitatively, we calculate the flight length distribution $\Gamma(\Delta x)$ of particles, where the flight length Δx is defined as the distance that a particle travels between two consecutive flips of the sign of its velocity. Particularly, for large Δx, the three different lattices types can be expected to deviate from one another, which we will explore in the following. Numerically, $\Gamma(\Delta x)$ is obtained by propagating $N = 2 \times 10^4$ particles up to $t_{\mathrm{max}} = 10^8 \times T$ with randomized initial velocities $-0.1 < v_0 < 0.1$, so all initial conditions would be located within the chaotic sea of the PL. The starting positions are chosen randomly within the interval $5 \times 10^8 + 10^3 < x_0/L < 5 \times 10^8 - 10^3$ and numerical convergence with respect to N and t_{max}, as well as independence from the choice of the initial positions, was checked very carefully. For the RL [Fig. 3(a)] we observe, to good approximation, for several orders of magnitude a power-law dependence $\Gamma(\Delta x) \propto (\Delta x)^{\alpha_{\mathrm{RL}}}$ with some exponent α_{RL}. In some sense, this simple power-law decay of $\Gamma(\Delta x)$ for the RL can be seen as a benchmark for the two other setups, as it represents the result for a completely uncorrelated lattice. Hence any deviations from $\Gamma(\Delta x)$ for the PL, and particularly for the FL, can be expected to relate to structural properties of the phase space of the corresponding lattice. In fact, the flight length distribution for the PL [Fig. 3(b)], while still

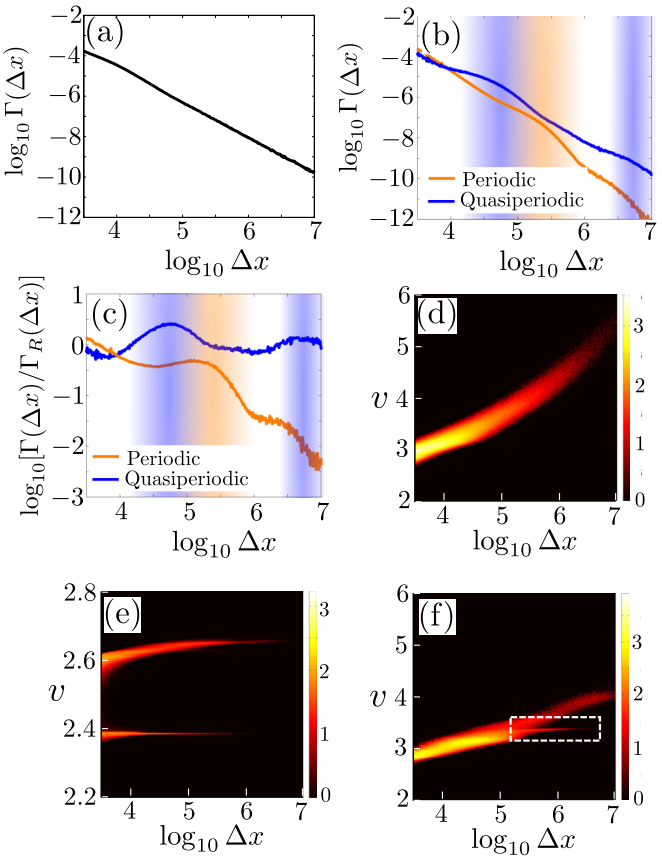

FIG. 3. (a) Flight length distribution $\Gamma(\Delta x)$ for large Δx in double logarithmic representation for the randomized lattice. (b) $\Gamma(\Delta x)$ for periodic and quasiperiodic lattice. Shaded intervals correspond to extraordinarily long flights. (c) Ratio of $\Gamma(\Delta x)$ of the periodic or quasiperiodic lattices and $\Gamma(\Delta x)$ of the randomized lattice. Shaded intervals are identical as in (b). Also shown are velocity-resolved flight length distributions $\Gamma(\Delta x, \bar{v})$ for the random (d), periodic (e), and quasiperiodic lattices (f). In the latter case, the dashed rectangle highlights the horizontal branch of long flights.

featuring an overall polynomial decay, also reveals deviations from the pure power-law-like behavior and shows a small amplitude oscillation around $5 \lesssim \log \Delta x \lesssim 5.5$. Interestingly, these deviations from the power-law-like decay of $\Gamma(\Delta x)$ can also be observed for the FL. This can be seen even clearer when calculating the ratio of $\Gamma(\Delta x)$ for the PL or the FL with respect to the RL [see Fig. 3(c)]. Here, in particular for the FL, pronounced maxima are apparent at distinct flight lengths, indicating that certain Δx are favored for the PL and the FL when comparing their flight length distributions to the one of the RL.

More insight into this effect can be obtained by calculating velocity resolved flight length distributions $\Gamma(\Delta x, \bar{v})$ [see Figs. 3(d), 3(e), and 3(f)], where $\bar{v}$ is the average velocity for a given flight of length Δx. [Similarly to the previous discussion, the time-reversal symmetry of the Hamiltonian ensures that $\Gamma(\Delta x, \bar{v}) = \Gamma(\Delta x, -\bar{v})$]. For the RL, we observe that $\Gamma(\Delta x, \bar{v})$ is concentrated around higher velocities for longer flight lengths Δx. This is in accordance with the observation made from the sample trajectories, namely that as soon as $|v| < |v^{\mathrm{C}}_{\mathrm{max}}|$ the velocity sign changes rapidly. Contrarily, once a particle reaches the high-velocity regime, the particles kinetic energy is large compared to the lattice potential and the influence of the lattice potential on the particles velocity can expected to be small. Hence the particle's velocity change upon collision with a barrier tends to be smaller the higher its velocity, which supports the effect of longer unidirectional flights at higher velocities. Apparently, for the PL this simple line of argument fails and $\Gamma(\Delta x, \bar{v})$ looks qualitatively different [see Fig. 3(e)], revealing that $\Gamma(\Delta x, \bar{v}) \neq 0$ only along two branches centered around $\bar{v} \approx 2.4$ and $\bar{v} \approx 2.6$, respectively. First, as there is an upper bound of $v^{\mathrm{C}}_{\mathrm{max}}$ on the particles velocity in the PL, this bound holds of course also for the average velocities $\bar{v}$ and hence $\Gamma(\Delta x, \bar{v}) = 0$ for $\bar{v} > v^{\mathrm{C}}_{\mathrm{max}}$ (keep in mind that the particle ensemble used to determine the flight length distributions is started with low energies and is hence located entirely within the chaotic sea). Second, the reason for the appearance of these two branches can be understood conveniently by considering again the systems PSS [Fig. 1(b)]. As mentioned above, long unidirectional flights in the PL are closely related to the stickiness of trajectories at regular structures which bound the chaotic sea. Apparently, there are notably two such regular structures present: the chain of three islands around $v \approx 2.5$ as well as the first invariant spanning curve (FISC) acting as an upper bound of the chaotic sea at around $v \approx 2.9$. Please note that the three islands should indeed be interpreted as a single regular structure, since they share a common central orbit with a periodicity of three unit cells. Indeed, one can check, by inspecting the corresponding trajectories, that the flights at large Δx around $\sim$2.4 are caused by particles getting sticky to the island chain, while the branch around $\sim$2.6 is caused by particles becoming sticky to the FISC. The fact that both branches in $\Gamma(\Delta x, \bar{v})$ appear to be at slightly smaller velocities than the associated regular structures has, in fact, a very simple explanation. For the PSS [Fig. 1(b)], the velocity of a particle is denoted at positions between scatterers and hence at positions where the potential is zero. While passing through the lattice, the particle has to surpass the repulsive barriers, and thus momentarily its kinetic energy is lowered. Hence the average velocity of a particle moving along some regular structure can indeed be expected to be smaller than the velocity suggested by the PSS as shown in Fig. 1(b).

Finally, lets turn our attention to the quasiperiodic case [Fig. 3(f)]. Again, $\Gamma(\Delta x, \bar{v})$ reveals the overall trend that longer flights possess larger average velocities, as already observed for the RL. Strikingly, we also see a horizontal branch centered around $\bar{v} \approx 3.2$, similarly to the two branches as observed for the PL. These, however, were remnants of regular structures of the PL's phase space, which—particularly in the case of regular islands—can be traced back to a synchronization of the particle motion with the lattice oscillation. As this, apparently, hinges on the periodicity of the lattice, it is now an intriguing question as to what is the cause of the horizontal branch in $\Gamma(\Delta x, \bar{v})$ of the FL.

V. TRANSIENT MOTION IN QUASIPERIODIC LATTICES

While for the PL, all the regular structures of the corresponding phase space can be investigated conveniently by means of the PSS, the same procedure cannot be applied to the FL, simply because the PSS inherently exploits the systems spatial periodicity. Hence, we must opt for a different approach and again turn to an observable related to the flight lengths. Here we calculate the flight length of a given initial condition (x_0, ϕ_0, v_0) by propagating particles until their velocity passes $v = 0$ for the first time. At this point, the modulus of the current position x of the particle minus x_0 gives the flight length $\Delta x(x_0, \phi_0, v_0)$ for this particular initial condition. The results for the PL, RL, and the FL are shown in Figs. 4(a), 4(b), and 4(c) respectively for an initial position $x_0 = 0$. For the PL, we very clearly see the counterparts of the regular structures as present in the PSS [cf. Fig. 1(b)]. If the trajectory is started within one of these structures, then it performs an

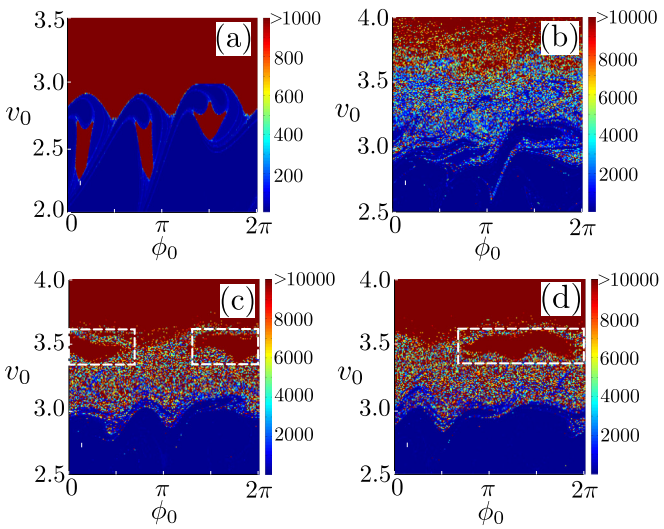

FIG. 4. Flight length $\Delta x(x_0, \phi_0, v_0)$ starting at $x_0 = 0$ as a function of the initial phase and initial velocity for the periodic (a), randomized (b), and quasiperiodic (c) lattice. (The shorter cutoff in the PL is for illustrative purpose only). In (d) we show $\Delta x(x_0 = 100 \times L, \phi_0, v_0)$ for the quasiperiodic case. Dashed rectangles highlight plateaus of extraordinarily long flights. Parameters are the same as in Fig. 2.

unidirectional motion through the lattice and $\Delta x(x_0,\phi_0,v_0)$ is, in fact, infinite. In this sense, calculating $\Delta x(x_0,\phi_0,v_0)$ can be seen simply as an alternative approach to determine the regular structures in the phase space of the PL. Its major advantage is that it does not intrinsically rely on the spatial periodicity of the system and can thus be applied for nonperiodic lattices also. Here, we, of course, have to keep in mind that $\Delta x(x_0,\phi_0,v_0)$ is expected to depend on x_0 and in particular does not obey $\Delta x(x_0,\phi_0,v_0) = \Delta x(x_0 \pm n \times L,\phi_0,v_0)$ as it does for the PL. Nevertheless, we will see that calculating the flight lengths for some exemplary x_0 for the RL and the FL does indeed reveal some valuable insight. Starting with the RL [Fig. 4(b)], we observe no apparent separation between regular and diffusive motion as seen in the PL, and, in fact, it is reasonable to assume that every trajectory will eventually pass $v = 0$, thus leading to a finite flight length Δx for all initial conditions. As a general trend, we again see that larger initial velocities v_0 tend to lead to longer flights, which agrees well with the discussion concerning the flight length distribution $\Gamma(\Delta x,\bar{v})$ [Fig. 3(d)]. Finally, for the FL [Fig. 4(c)], $\Delta x(0,\phi_0,v_0)$ qualitatively differs from both the periodic and the randomized cases. Here we see a sharp increase of the flight length at around $v_0 \sim 3$. Furthermore, we see a plateau of extraordinarily long flights centered around $\phi_0 \sim 0/2\pi$ and $v_0 \sim 3.5$, which is very much reminiscent of the regular islands as seen for the PL. Interestingly, like the regular islands in the PL, the plateau falls together with a horizontal branch in the flight lengths distribution $\Gamma(\Delta x,\bar{v})$ as shown in Fig. 3(f) [for the same reason as before, the plateaus' velocity in $\Delta x(0,\phi_0,v_0)$ appears slightly higher than the velocity of the corresponding branch in $\Gamma(\Delta x,\bar{v})$]. At this point, the question arises regarding how $\Delta x(x_0,\phi_0,v_0)$ changes upon changing x_0. Exemplarily, we show the result for $x_0 = 100 \times L$ in Fig. 4(d), revealing that the observed plateau appears again within the same velocity interval but centered around a different phase. By repeating this for various x_0 we can convince ourselves that the appearance of a plateau of long flights at velocities of $v_0 \sim 3.5$ seems to be a "global" property of the FL rather than a peculiarity for some distinct parts of the lattice. Despite the similarities between the plateau as observed in the FL and the regular islands in the PL, there is also a major difference, which is the finite flight length within the FL even for trajectories started within the plateau, thus making this a phenomenon of a transient dynamics.

Lets us briefly summarize what we know about the motion in the FL so far: Apparently, we have found domains of initial conditions leading to exceptionally long unidirectional flights. In particular, these defy the simple overall trend of longer flights for higher velocities, thereby contrasting the dynamics in the RL. Additionally, the flight lengths remain finite, which—in turn—is in contrast to motion on a ballistic island of the PL. However, all the described features are reminiscent of a stickiness event of a trajectory in the PL. Hence, it appears as if trajectories in the FL would follow some phase-space structure to which they become sticky for a long time but are eventually able to escape. Naturally, the question arises regarding what this phase-space structure is and what is its physical origin and, maybe more importantly, if we can somehow deduce and understand is location around $v \sim 3.5$ (and $\phi \sim 0$ for $x_0 = 0$).

VI. BLOCK DECOMPOSITION OF THE FIBONACCI LATTICE

At this point, we need to make use of some distinct properties of the FL. In particular, we will argue that it can be decomposed into building blocks on various hierarchical levels. Based on this block decomposition of the FL, we will construct a set of PSS of periodic lattices and their corresponding Poincaré maps, which govern the dynamics in the FL on different length scales. Finally, we show how invariant subsets of these Poincaré maps are related directly to the observed long ballistic flight events.

A. Poincaré maps and their application to randomized systems

For the PL, we defined the Poincaré surfaces to be at positions $X^{\mathrm{PSS}} = \{x,\ x = n \times L\}$ for $n \in \mathbb{N}$ [cf. Fig. 1(a)]. Subsequent coordinates on these surfaces of a trajectory moving through the lattice are then linked via the Poincaré map:

$$(\phi_{k+1},v_{k+1}) = \mathcal{M}_{\mathcal{A}}(\phi_k,v_k), \tag{4}$$

which is thus determined implicitly by the scattering properties of the lattice barriers (the subscript "$\mathcal{A}$" denotes that, as before, the PL consists of $\mathcal{A}$-type barriers). Note that dynamical processes occurring on length scales below the distance of adjacent Poincaré surfaces are not resolved by $\mathcal{M}_{\mathcal{A}}$ for the given choice of the surfaces. For example, orbits trapped between two positions of adjacent Poincaré surfaces which are present even for oscillating repulsive barriers (see Ref. [36]) are not captured (but these are also not relevant for our work). The main features of $\mathcal{M}_{\mathcal{A}}$ can be read off directly from the setups PSS [Fig. 1(b)]. Particularly, a stable fixed point (ϕ_f,v_f) of a given period p:

$$(\phi_f,v_f) = \mathcal{M}_A^p(\phi_f,v_f), \tag{5}$$

where the superscript denotes a p-fold application of $\mathcal{M}_A$, is made apparent as p regular islands in the PSS. Thereby, each of the fixed point surrounding closed curves constitutes an invariant set under the action of $\mathcal{M}_A^p$.

Equivalently, we can describe the dynamics in nonperiodic lattices by means of successive applications of the Poincaré maps $\mathcal{M}_A$ and $\mathcal{M}_B$. An intriguing question is now whether a randomized lattice may allow for periodic motion on the level of Poincaré maps. One straightforward way this could be realized is by demanding that $\mathcal{M}_A$ and $\mathcal{M}_B$ share a common fixed point: $(\phi_f,v_f) = \mathcal{M}_A(\phi_f,v_f) = \mathcal{M}_B(\phi_f,v_f)$. If such a point exists, then one might say that (ϕ_f,v_f) constitutes a fixed point of the dynamics in the entire nonperiodic lattice. While by fine-tuning of parameters it might indeed be possible to match fixed points of $\mathcal{M}_A$ and $\mathcal{M}_B$, in a generic setting this cannot be expected to happen. Also, even if such a point exists, in order for it to be stable, the surrounding invariant sets of $\mathcal{M}_A$ and $\mathcal{M}_B$ would also have to be invariant under the action of both $\mathcal{M}_A$ and $\mathcal{M}_B$. This seems to be even harder to accomplish by means of fine-tuning parameters and in fact we see no such stable fixed points in both studied nonperiodic cases. Finally, for nonperiodic lattices, fixed points of $\mathcal{M}_A$ or $\mathcal{M}_B$ of order $p > 1$, corresponding to ballistic unbounded motion, are not relevant as these would require a repeating sequence of $\mathcal{A}$ and $\mathcal{B}$ barriers.

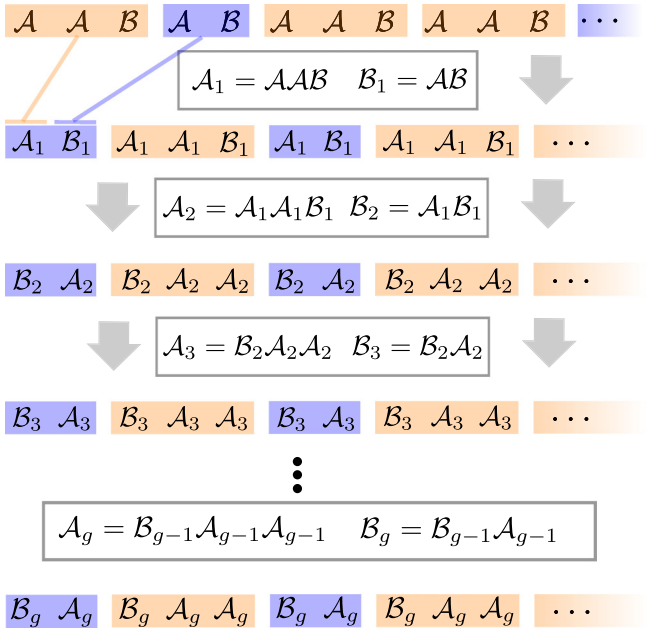

FIG. 5. Block decomposition of the Fibonacci lattice in symbolic notation according to the decomposition rule given in Eqs. (6) and (7). The first row depicts the first few elements of the Fibonacci sequence [cf. Eq. (3), where a 1 (0) corresponds to a barrier of type $\mathcal{A}$ ($\mathcal{B}$)]. At the same time, this first row is the "zeroth generation" of the decomposition hierarchy. All further rows show block decompositions of increasing generations.

B. Symmetry adopted Poincaré maps of the Fibonacci lattice

Naively, one might argue that in order for the FL to support ballistic islands, again one would have to match fixed points of $\mathcal{M}_A$ and $\mathcal{M}_B$ and their invariant subsets. As we will see in the following, this is, however, too simplistic and the FL requires a more sophisticated analysis. At this point, we would like to stress that we checked the validity of the numerical results, presented in the following, beyond the for this manuscript relevant scales.

The key idea is to realize that the FL can be decomposed into building blocks as illustrated in Fig. 5. In the first decomposition, we define the building blocks to be $\mathcal{A}_1 \equiv \mathcal{A}\mathcal{A}\mathcal{B}$ and $\mathcal{B}_1 \equiv \mathcal{A}\mathcal{B}$. If we again focus on unbounded motion, then we can now describe the dynamics on the level of the Poincaré maps $\mathcal{M}_{\mathcal{A}_1}$ and $\mathcal{M}_{\mathcal{B}_1}$, which iterate trajectories between positions between adjacent blocks. This decomposition can be continued, by defining the "next generations" of blocks as:

$$\mathcal{A}_g = \mathcal{A}_{g-1}\mathcal{A}_{g-1}\mathcal{B}_{g-1},\ \mathcal{B}_g = \mathcal{A}_{g-1}\mathcal{B}_{g-1} \text{ for } g \leqslant 2, \quad (6)$$

$$\mathcal{A}_g = \mathcal{B}_{g-1}\mathcal{A}_{g-1}\mathcal{A}_{g-1},\ \mathcal{B}_g = \mathcal{B}_{g-1}\mathcal{A}_{g-1} \text{ for } g > 2, \quad (7)$$

with the corresponding Poincaré maps $\mathcal{M}_{\mathcal{A}_g}$ and $\mathcal{M}_{\mathcal{B}_g}$ and with $\mathcal{A}_0 \equiv \mathcal{A}$ and $\mathcal{B}_0 \equiv \mathcal{B}$. Hence, the FL allows for unbounded regular motion if two Poincaré maps of any given generation feature two identical regular structures (in contrast to the RL, where only the two maps for $g = 0$ are relevant).

The invariant subsets of the Poincaré maps of any generation can be visualized conveniently by means of the PSS of the corresponding periodic system (e.g., $\mathcal{A}_g\mathcal{A}_g\mathcal{A}_g\ldots$) with

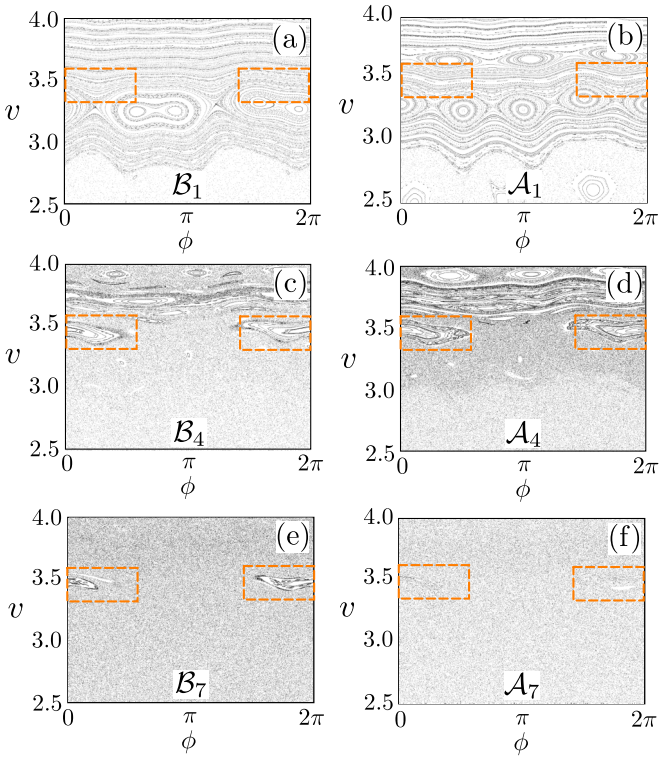

FIG. 6. Poincaré surfaces of section of lattices consisting of periodic repetitions of blocks: $\mathcal{B}_1$ (a), $\mathcal{A}_1$ (b), $\mathcal{B}_4$ (c), $\mathcal{A}_4$ (d), $\mathcal{B}_7$ (e), and $\mathcal{A}_7$ (f). Dashed rectangles are at the same locations as in Fig. 4(c) denoting a domain of long flights in the quasiperiodic lattice. Remaining parameters are as in Fig. 2.

Poincaré surfaces between each adjacent building blocks. While the "zeroth generation" PSS corresponding to $\mathcal{A}_0$ is already shown in Fig. 1(b), some of the relevant PSS of various higher generations are shown in Fig. 6. We find that the PSS of blocks of some generations feature indeed a regular island around the same phase-space coordinates as the plateau of long ballistic flights as observed in the FL [cf. Fig. 4(c)].

In order to understand how these regular structures are linked with the long flights in the FL, let us consider the PSS corresponding to $\mathcal{A}_4$ and $\mathcal{B}_4$ [Figs. 6(c) and 6(d)]. For example, a trajectory starting at $x_0 = 0$ and with (ϕ_0, v_0) corresponding exactly to the fixed point centering the regular island of $\mathcal{M}_{\mathcal{B}_4}$ will pass the first surface of section at $x = 34 \times L$ (as this is the length of one $\mathcal{B}_4$ block) with the same coordinates $(\phi_1, v_1) = (\phi_0, v_0)$. The next block is of type $\mathcal{A}_4$ (and thus of length $55 \times L$) and, consequently, the coordinates on the next Poincaré surface at $x = 89 \times L$ are given by $(\phi_2, v_2) = \mathcal{M}_{\mathcal{A}4}(\phi_1, v_1)$. Even though (ϕ_1, v_1) does not correspond exactly to the fixed point of $\mathcal{M}_{\mathcal{A}_4}$, it does correspond to one of the invariant curves of the surrounding regular island and hence the trajectory will surpass the block confined to this particular invariant curve. Because the regular islands of both maps $\mathcal{M}_{\mathcal{A}_4}$ and $\mathcal{M}_{\mathcal{B}_4}$ are rather similar to one another, we can expect that the trajectory needs many such iterations before it can finally leave this particular domain of phase space, which ultimately causes the observed stickiness and, equally, the long ballistic flights at this particular velocity domain.

Even though one may describe the dynamics on different lengths scales in the FL by means of any of the possible decompositions, we see that only the PSSs of blocks of some particular generations contain notable common regular structures which then relate to domains of extraordinarily long ballistic flights. We find, numerically, that the appearance of similar regular structures in the PSS of $\mathcal{A}_g$ and $\mathcal{B}_g$ is suppressed more strongly with increasing g with an increasing difference in the potential heights $V_\mathcal{A}$ and $V_\mathcal{B}$. In this way, one may, to some extent, choose which of the generations of the decomposition support long ballistic flights in the FL and thus also manipulate the length scale of these long flight events. For example, we find that by setting $V_\mathcal{A} = 1.5$ as before and $V_\mathcal{B} = 0.1$ (instead of $V_\mathcal{B} = 1.0$), the two maxima in the flight length distribution in the FL [as shown in Fig. 3(c)] are shifted by roughly one order of magnitude to smaller Δx as compared to the case of $V_\mathcal{B} = 1.0$. Additionally, the regular structures in the hierarchical PSSs decay approximately one generation earlier, matching the observation of the shorter preferred length scale in the flight length distribution.

VII. CONCLUSION

We have investigated the chaotic dynamics of classical particles exposed to a periodically driven, spatially quasiperiodic lattice potential. As two points of reference, we compare our results to periodic- and fully randomized lattices and indeed find unique features of the particle dynamics for the quasiperiodic lattice. Specifically, we show that particles perform exceptionally long ballistic flights at distinct velocities. Since the usual tools as commonly applied in the investigation of periodic systems, such as Poincaré surfaces of sections, intrinsically rely on the spatial periodicity of the system, they cannot be applied straightforwardly here. However, we show how a suitable set of Poincaré surfaces of periodic lattices provides the decisive insights into the dynamics of the quasiperiodic lattice. These Poincaré surfaces and their corresponding Poincaré maps are introduced naturally to the system by an underlying hierarchy of block decompositions of the lattice. Thereby, each Poincaré map associated to a decomposition of a given level of the hierarchy describes the particle dynamics on a different length scale and we show how regular structures of these maps translate directly into the observed domains of long ballistic flights in the quasiperiodic lattice. Even though the block decompositions work up to arbitrarily large length scales, which of these scales are actually of relevance to the dynamics is determined by the scattering properties of the individual barriers constituting the lattice. Hence, the shown results are caused by an intricate interplay of the global structures of the quasiperiodic lattice on the one hand and of the "local" scattering properties of individual barriers on the other hand.

ACKNOWLEDGMENTS

We thank B. Liebchen for many helpful discussions.

[1] P. Hänggi and F. Marchesoni, Artificial Brownian motors: Controlling transport on the nanoscale, Rev. Mod. Phys. **81**, 387 (2009).
[2] S. Denisov, S. Flach, and P. Hänggi, Tunable transport with broken spacetime symmetries, Phys. Rep. **538**, 77 (2014).
[3] V. Serreli, C. F. Lee, E. R. Kay, and D. A. Leigh, A molecular information ratchet, Nature **445**, 523 (2007).
[4] S. Matthias and F. Müller, Asymmetric pores in a silicon membrane acting as massively parallel brownian ratchets, Nature **424**, 53 (2003).
[5] P. Reimann, Brownian motors: Noisy transport far from equilibrium, Phys. Rep. **361**, 57 (2002).
[6] R. D. Astumian and M. Bier, Fluctuation Driven Ratchets: Molecular Motors, Phys. Rev. Lett. **72**, 1766 (1994).
[7] D. Cubero and F. Renzoni, Hidden Symmetries, Instabilities, and Current Suppression in Brownian Ratchets, Phys. Rev. Lett. **116**, 010602 (2016).
[8] R. K. Schmitt, J. M. R. Parrondo, H. Linke, and J. Johansson, Molecular motor efficiency is maximized in the presence of both power-stroke and rectification through feedback, New J. Phys. **17**, 065011 (2015).
[9] R. D. Astumian, Thermodynamics and kinetics of a Brownian motor, Science **276**, 917 (1997).
[10] S. Savelev, V. Misko, F. Marchesoni, and F. Nori, Separating particles according to their physical properties: Transverse drift of underdamped and overdamped interacting particles diffusing through two-dimensional ratchets, Phys. Rev. B **71**, 214303 (2005).
[11] L. Bogunovic, R. Eichhorn, J. Regtmeier, D. Anselmetti, and P. Reimann, Particle sorting by a structured microfluidic ratchet device with tunable selectivity: Theory and experiment, Soft Matter **8**, 3900 (2012).
[12] J. S. Roth, Y. Zhang, P. Bao, M. R. Cheetham, X. Han, and S. D. Evans, Optimization of Brownian ratchets for the manipulation of charged components within supported lipid bilayers, Appl. Phys. Lett. **106**, 183703 (2015).
[13] M. A. Tahir, F. Nori, and B. B. Yellen, Dynamically-tunable colloidal band-pass and band-gap filters, J. Appl. Phys. **115**, 134902 (2014).
[14] M. Sadgrove, T. Schell, K. Nakagawa, and S. Wimberger, Engineering quantum correlations to enhance transport in cold atoms, Phys. Rev. A **87**, 013631 (2013).
[15] D. H. White, S. K. Ruddell, and M. D. Hoogerland, Experimental realization of a quantum ratchet through phase modulation, Phys. Rev. A **88**, 063603 (2013).
[16] R. Gommers, S. Denisov, and F. Renzoni, Quasiperiodically Driven Ratchets for Cold Atoms, Phys. Rev. Lett. **96**, 240604 (2006).
[17] A. Wickenbrock, P. C. Holz, N. A. Abdul Wahab, P. Phoonthong, D. Cubero, and F. Renzoni, Vibrational Mechanics in an Optical Lattice: Controlling Transport via Potential Renormalization, Phys. Rev. Lett. **108**, 020603 (2012).
[18] N. V. Alexeeva, I. V. Barashenkov, and G. P. Tsironis, Impurity-Induced Stabilization of Solitons in Arrays of Parametrically Driven Nonlinear Oscillators, Phys. Rev. Lett. **84**, 3053 (2000).

[19] G. Yu, X. Wang, and Z. Tao, Resonant emission of solitons from impurity-induced localized waves in nonlinear lattices, Phys. Rev. E **83**, 026605 (2011).
[20] Y. Braiman, John F. Lindner, and William L. Ditto, Taming spatiotemporal chaos with disorder, Nature **378**, 465 (1995).
[21] Y. Lei and F. Guan, Disorder induced order in an array of chaotic duffing oscillators, Int. J. Mod. Phys. C **23**, 1250071 (2012).
[22] T. Wulf, B. Liebchen, and P. Schmelcher, Disorder Induced Regular Dynamics in Oscillating Lattices, Phys. Rev. Lett. **112**, 034101 (2014).
[23] F. Bloch, Über die Quantenmechanik der Elektronen in Kristallgittern, Z. Phys. **52**, 555 (1929).
[24] P. W. Anderson, Local moments and localized states, Rev. Mod. Phys. **50**, 191 (1978).
[25] D. Shechtman, I. Blech, D. Gratias, and J. W. Cahn, Metallic Phase with Long-Range Orientational Order and no Translational Symmetry, Phys. Rev. Lett. **53**, 1951 (1984).
[26] K. Iguchi, Theory of quasiperiodic lattices. I. Scaling transformation for a quasiperiodic lattice, Phys. Rev. B **43**, 5915 (1991).
[27] M. Kohmoto, L. P. Kadanoff, and C. Tang, Localization Problem in one Dimension: Mapping and Escape, Phys. Rev. Lett. **50**, 1870 (1983).
[28] M. Kohmoto, B. Sutherland, and C. Tang, Critical wave functions and a Cantor-set spectrum of a one-dimensional quasicrystal model, Phys. Rev. B **35**, 1020 (1987).
[29] E. Maciá, On the nature of electronic wave functions in one-dimensional self-similar and quasiperiodic systems, ISRN Condens. Matter Phys. **2014**, 165943 (2014).
[30] W. Zhi-Xiong and W. Zhi-Ying, Some properties of the singular words of the Fibonacci word, Eur. J. Combin. **15**, 587 (1994).
[31] X. Droubay, Palindromes in the Fibonacci word, Inform. Process. Lett. **55**, 217 (1995).
[32] C. Morfonios, P. Schmelcher, P. A. Kalozoumis, and F. K. Diakonos, Local symmetry dynamics in one-dimensional aperiodic lattices: A numerical study, Nonlin. Dynam. **78**, 71 (2014).
[33] C. Li, X. Zhang, and Z. Cao, Triangular and Fibonacci number patterns driven by stress on core/s microstructures, Science **309**, 909 (2005).
[34] A. J. Lichtenberg and M. A. Lieberman, *Regular and Chaotic Dynamics*, Applied Mathematical Sciences, Vol. 38 (Springer, New York, 1992).
[35] A. K. Karlis, P. K. Papachristou, F. K. Diakonos, V. Constantoudis, and P. Schmelcher, Fermi acceleration in the randomized driven Lorentz gas and the Fermi-Ulam model, Phys. Rev. E **76**, 016214 (2007).
[36] F. R. N. Koch, F. Lenz, C. Petri, F. K. Diakonos, and P. Schmelcher, Dynamical trapping and chaotic scattering of the harmonically driven barrier, Phys. Rev. E **78**, 056204 (2008).